Rotational perturbation to the natural-parity rotational band of ^{163}Dy

M. Oshima, E. Minehara, and S. Kikuchi
Japan Atomic Energy Research Institute, Tokai, Ibaraki 319-11, Japan

T. Inamura and A. Hashizume
The Institute of Physical and Chemical Research (RIKEN), Wako, Saitama 351-01, Japan

H. Kusakari
Faculty of Education, Chiba University, Yayoi, Chiba 260, Japan

M. Matsuzaki*
Department of Physics, Kyoto University, Kyoto 606, Japan
(Received 26 July 1988)

Reduced transition probabilities of $B(M1)$ and $B(E2)$ are determined up to spin $\frac{23}{2}$ on the basis of a Coulomb excitation experiment. Strong signature-dependent staggering was observed for $\Delta I=1$ $M1$ transition probabilities. In contrast, there was no significant signature dependence observed for $\Delta I=1$ and $\Delta I=2$ $E2$ transition probabilities as well as for level energies. We carried out a rotating-shell-model calculation with the γ degree of freedom. The origin of the unexpected signature dependence of the $B(M1)$ is shown to be due to the characteristic coherence between the orbital and the spin contributions. We also show that the coupling with the γ-vibrational phonons makes it possible to reproduce the absolute values of the $B(M1)$ at high-spin states without using the phenomenological g_R. Both the stretched and nonstretched $B(E2)$'s are well reproduced in the rotating shell model without assuming triaxiality.

I. INTRODUCTION

Recently, electromagnetic transition probabilities in rotational bands have been studied[1-7] extensively and considerable data are being accumulated. Signature dependence of the reduced transition probabilities which originates from the Coriolis force has been found to provide a sensitive test of the wave functions. Such a signature dependence has drawn much attention to the γ degrees of freedom in the rotating nuclear system.[8-12] Since the Coriolis force strongly acts on particles in high-spin orbitals, most experimental and theoretical studies are concerned with rotational bands based on them.

In contrast, the rotational perturbation to lower-spin orbitals has not been studied well because the effects are believed to be rather weak. It is, however, desirable to study in detail how the Coriolis force affects the rotational bands based on the lower-spin orbitals, such as $h_{9/2}$ or $f_{7/2}$. For this purpose we made an experiment to determine reduced transition probabilities in ^{163}Dy whose ground-state rotational band is based on such low-spin orbitals and reported an unexpected signature dependence of the $B(M1)$ values.[13] A simple rule for the signature dependence, which has been well established for the high-spin-orbital bands,[14] was found not to hold.

Since the low-spin-orbital bands have a natural parity in nature, j-mixing is the most distinct property of these bands. This feature as well as the γ degrees of freedom may be related to the unexpected signature dependence of the $B(M1)$. Therefore, in order to understand the experimental results of ^{163}Dy, we have employed a rotating shell model within which one can treat the j-mixing, dynamical γ deformation, and also static γ deformation.[8,9] In this paper we shall describe details of the experiment which was not included in the previous paper,[13] and of the rotating-shell-model calculation.

The ground-state rotational band of ^{163}Dy has been investigated so far through Coulomb excitation by light ions.[15-17] From these works the ground band has been known up to $I=\frac{17}{2}$.[15,18] Lifetimes of the ground-band members were deduced only up to the 2nd excited state $\frac{9}{2}^-$ from the Coulomb-excitation experiments.[16,17]

II. EXPERIMENTAL PROCEDURES AND RESULTS

As was previously reported,[13] we made a multiple Coulomb-excitation experiment on ^{163}Dy: $\gamma\gamma$ coincidences, γ-ray angular distributions, and Doppler-broadened γ-ray line shapes were measured. The data acquisition was controlled by a PDP-11 computer and list-mode data of 1.4×10^8 coincidence events were recorded on magnetic tapes for later analysis. The proposed level scheme[13] of the ground-state rotational band of ^{163}Dy is shown in Fig. 1.

Figure 2 shows the Compton-suppressed γ-ray singles spectrum measured at 0° to the beam. Since the γ-ray line shape due to the Doppler broadening depends on the measured angles relative to the beam axis especially at high energies, special care was taken in analyzing the γ-

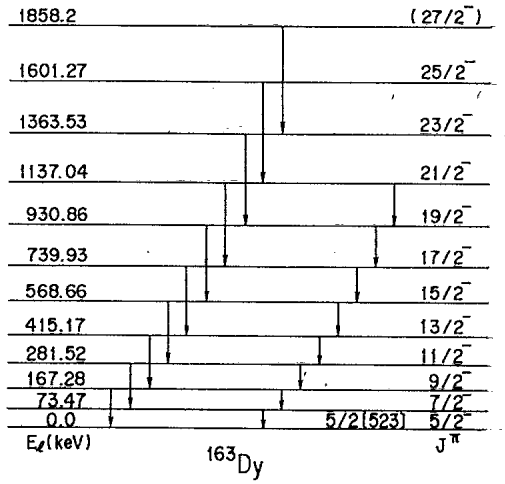

FIG. 1. A level scheme of the ground-state rotational band of ^{163}Dy.

ray angular distributions: γ-ray intensity was obtained as a total area of the stopped and Doppler-broadened part; the detection efficiency was estimated at the centroid energy of the line shapes. Derived angular-distribution coefficients, A_2 and A_4, are summarized in Table I of Ref. 13.

$E2/M1$ mixing ratios of $\Delta I=1$ transition have been extracted from the experimental angular distributions. A typical example of the mixing-ratio analysis is shown in Fig. 3. Relatively small uncertainties of the A_4 as well as the A_2 make it possible to deduce the $E2/M1$ mixing ratio unambiguously: The candidate of mixing ratio with a small absolute value is excluded as shown in Fig. 3. It should be noted that the absolute values are exceptionally large, $|\delta| \geq 1.7$, reflecting weak $M1$ components. We have reanalyzed the data and revised four sets of A_2 and A_4 values in Table I of Ref. 13: $A_2=+0.02(4)$ and $A_4=0.00(5)$ for the $\frac{9}{2}\rightarrow\frac{5}{2}$ transition; $-0.160(21)$ and $+0.05(6)$ for the $\frac{11}{2}\rightarrow\frac{9}{2}$; $-0.210(20)$ and $+0.047(23)$ for the $\frac{13}{2}\rightarrow\frac{11}{2}$; $-0.39(3)$ and $+0.052(21)$ for the $\frac{15}{2}\rightarrow\frac{13}{2}$. The derived mixing ratios are $-1.7(3)$, $-2.9(3)$, $-1.65(25)$, and $-1.7(5)$ for the $\frac{11}{2}\rightarrow\frac{9}{2}$, $\frac{13}{2}\rightarrow\frac{11}{2}$, $\frac{15}{2}\rightarrow\frac{13}{2}$, and $\frac{19}{2}\rightarrow\frac{17}{2}$ transitions, respectively: The centroid values have not changed significantly but the uncertainties were reevaluated as one standard deviation.

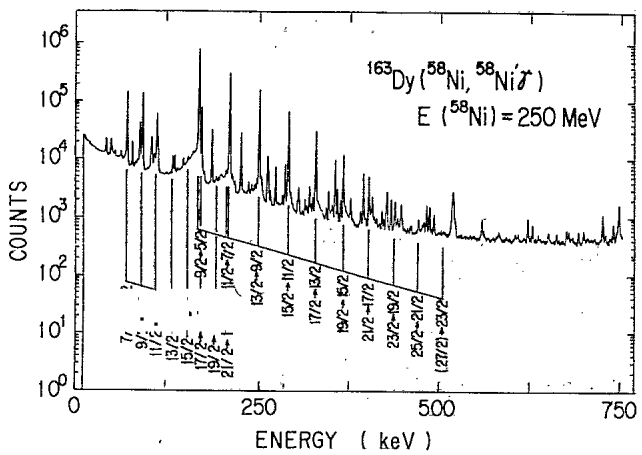

FIG. 2. A Compton-suppressed singles γ-ray spectrum measured at 0° to the beam.

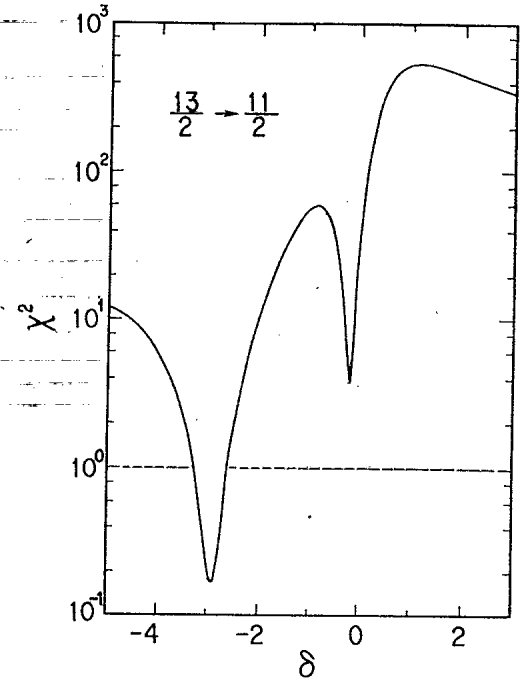

FIG. 3. A typical example of γ-ray angular distribution analysis for the $\frac{13}{2}^-\rightarrow\frac{11}{2}^-$ transition. The reduced χ^2 is plotted as a function of $E2/M1$ mixing ratio δ. The uncertainty was estimated for a 67% confidence level (1 standard deviation) shown with a broken line in the figure.

The experimental line shapes were fitted with theoretical line shapes calculated by a computer program SHAPES (Ref. 19) which included the effects of angular distribution of recoiling nuclei, feeding from higher-lying levels, and the finite size of the germanium detector. The line shapes are integrated over the degrading projectile energy because the target was thick enough to stop the recoil. Up to spin $\frac{23}{2}$ the feedings from unobserved higher-spin states were taken from the predictions of the Winther–de Boer code using rotational matrix elements. Analysis proceeded from the highest-spin transition observed. This experimental result was then applied in analyzing the next highest transition, and so on down the bands. More detailed formulation of the analysis is described in Ref. 19. The line-shape analyses for the states from the $\frac{13}{2}^-$ to the $\frac{23}{2}^-$ are shown in Fig. 4. Intruder γ rays which were obviously not part of the line-shape structure were excluded from the χ^2 of the fit. These points are indicated by open circles in Fig. 4. The lifetimes obtained are summarized in Table I.

The absolute transition probabilities $B(M1;I\rightarrow I-1)$, $B(E2;I\rightarrow I-1)$, and $B(E2;I\rightarrow I-2)$ are deduced from the nuclear lifetimes, the γ-ray branching ratios, and the $E2/M1$ mixing ratios. They are summarized in Table I and are plotted in Figs. 5–7. In the present line-shape

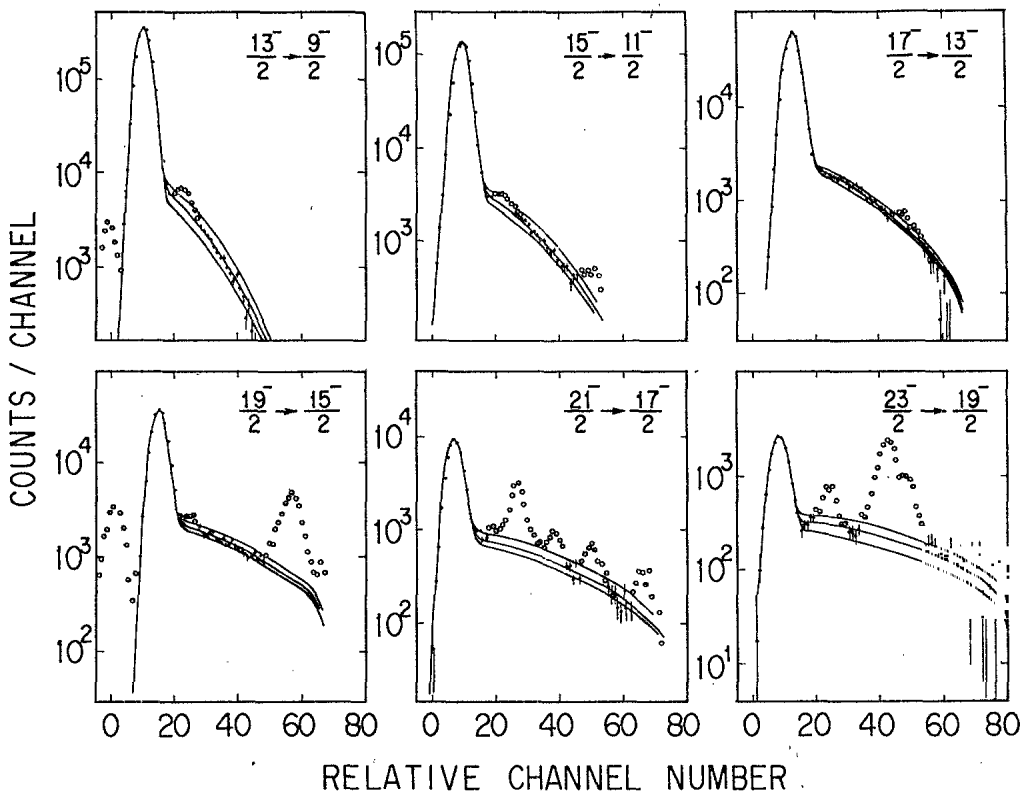

FIG. 4. Results of line-shape analyses. Dots with error bars are included in the fitting. The open circles are neglected in the fit because there are considerable effects from intruder γ rays. Solid curves represent the best fits and the range of uncertainties.

measurement, the nuclear lifetime for the $\frac{11}{2}^-$ state was not determined, because it was found too long to be extracted from the line-shape analysis. The values for $I=\frac{11}{2}$ indicated by open circles in Figs. 5 and 6 were estimated as follows. The $B(E2;I\rightarrow I-2)$ values for $I=\frac{9}{2},\frac{13}{2}-\frac{23}{2}$ (Fig. 7) are close to the prediction of the Bohr-Mottelson strong-coupling model,[20] i.e.,

$$B(E2;I\rightarrow I-2)=\frac{5}{16\pi}\langle I2K0|I-2K\rangle^2 Q_t^2 , \qquad (1)$$

where we assume transition quadrupole moments as $Q_t=7.2$ b. We estimated the $B(M1;\frac{11}{2}\rightarrow\frac{9}{2})$ and $B(E2;\frac{11}{2}\rightarrow\frac{9}{2})$ values using the experimental γ-ray branching, mixing ratio, and $Q_t=7.2$ b.

TABLE I. Summary of reduced transition probabilities.

I	τ (ps)	$B(M1;I\rightarrow I-1)$ (μ_N^2)	$B(E2;I\rightarrow I-1)$ (e^2b^2)	$B(E2;I\rightarrow I-2)$ (e^2b^2)
$\frac{7}{2}$	2180(70)		1.97(8)[a]	
$\frac{9}{2}$	520(30)	0.0013(7)[b]	1.47(17)[b]	0.540(11)[a]
$\frac{11}{2}$		[0.0031(8)][c]	[0.98(10)][c]	[0.88][c]
$\frac{13}{2}$	66(26)	0.0013(6)	0.87(35)	1.10(44)
$\frac{15}{2}$	25(5)	0.0039(12)	0.64(14)	1.51(31)
$\frac{17}{2}$	16(2)	0.0009(5)	0.33(8)	1.32(18)
$\frac{19}{2}$	9.0(10)	0.0021(13)	0.23(11)	1.4(4)
$\frac{21}{2}$	6.0(10)			1.32(24)
$\frac{23}{2}$	4.3(8)			1.23(35)

[a]From Ref. 16.
[b]From Ref. 18.
[c]Obtained by assuming that the $B(E2;11/2\rightarrow 7/2)$ is equal to the prediction of the Bohr-Mottelson strong-coupling model (see text).

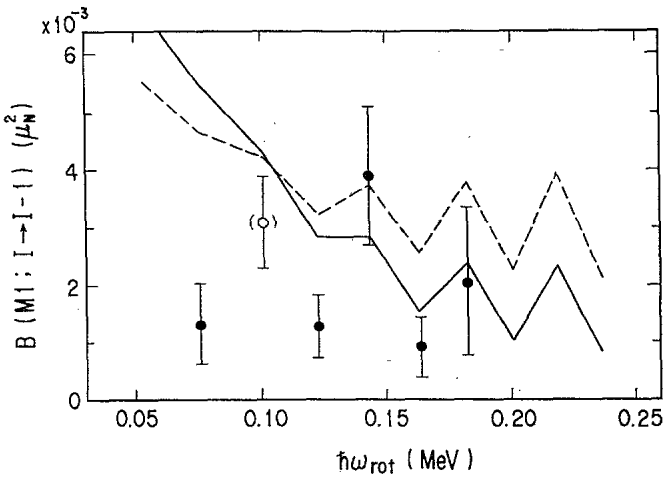

FIG. 5. $B(M1;I\rightarrow I-1)$ values for the ground-state rotational band of ^{163}Dy. The solid (broken) line shows the calculation with (without) the γ vibrations. The experimental value for $I=\frac{11}{2}$ was obtained by assuming $Q_t=7.2$ b (see discussions in text). The calculated values of g_{RPA} are about 0.34 which is almost independent of $\hbar\omega_{\mathrm{rot}}$ because we used the diabatic representation [see Fig. 2 of Ref. 9].

Quasineutron energy splitting $E_{+i}-E_{-i}$ was deduced from the experimental level energies and is plotted as a function of $\hbar\omega_{\mathrm{rot}}$ in Fig. 8. It should be emphasized that the energy splitting is very small as compared with the ones for the $\nu i_{13/2}$ and $\pi h_{11/2}$ orbital bands.[1-7] On the other hand, the $B(M1;I\rightarrow I-1)$ values show a strong signature-dependent staggering. The small energy splitting and the large signature dependence of the $B(M1)$ take place simultaneously in ^{163}Dy. This is different from the case of high-j orbitals, where the signature dependence of the $B(M1)$ values is generally known to be correlated with the signature-dependent energy splitting.[1-7] It should also be noted that so far no significant signature dependence of the $B(M1)$ has been observed for bands built on such a natural-parity low-spin orbital as $f_{7/2}$ or $h_{9/2}$ with $\Omega\neq\frac{1}{2}$.

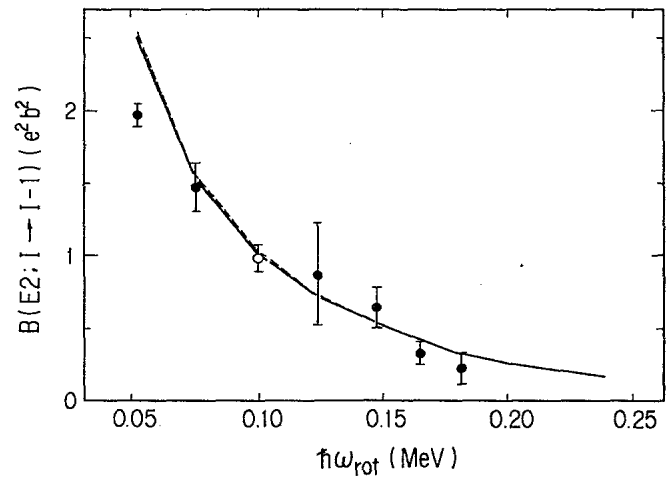

FIG. 6. $B(E2;I\rightarrow I-1)$ values for the ground-state rotational band of ^{163}Dy. The theoretical values were obtained using an aligned angular momentum $i_x=1.0$. The notations for the solid and broken lines are the same as in Fig. 5. The experimental value for $I=\frac{11}{2}$ was obtained by assuming $Q_t=7.2$ b (see discussions in text).

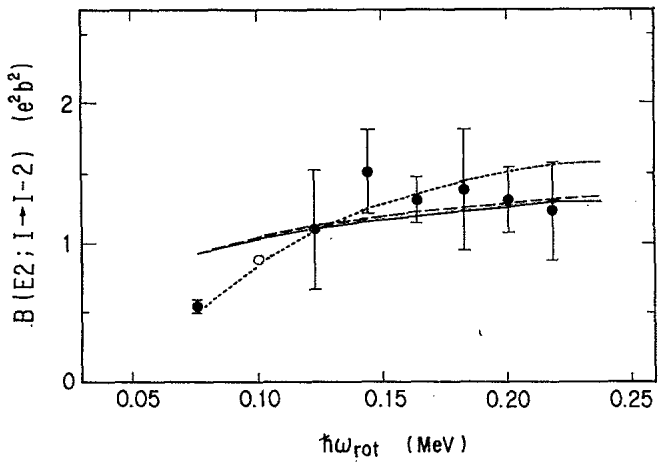

FIG. 7. $B(E2;I\rightarrow I-2)$ values for the ground-state rotational band of ^{163}Dy. The notations for the solid and broken lines are the same as in Fig. 5. The dotted line indicates the prediction of the Bohr-Mottelson strong-coupling model (Ref. 20) for $Q_t=7.2$ b (see discussions in text).

In order to understand the present experimental results, we made theoretical calculations based on the rotating shell model.

III. THEORETICAL CALCULATION

A. Rotating shell model and γ degrees of freedom

We performed a microscopic theoretical calculation based on the rotating shell model.[8,9] Expansion of the D functions in $1/I$ enables us to calculate transition rates

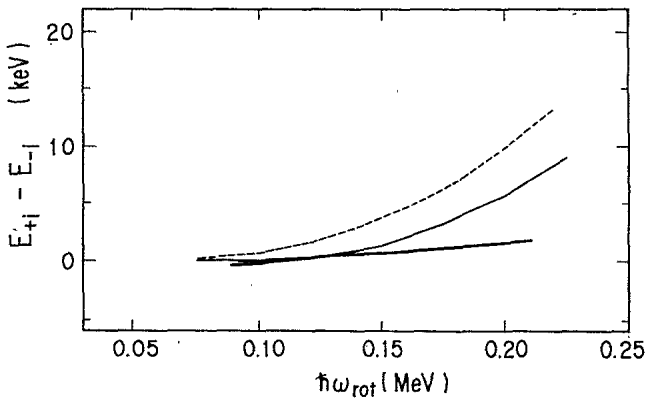

FIG. 8. Quasineutron energy splitting $E_{+i}-E_{-i}$ plotted as a function of $\hbar\omega_{\mathrm{rot}}$. The bold line indicates the experimental data. The solid (broken) line shows the calculation with (without) the γ vibrations. Here, the solid line is the result of the parabolic smoothing in order to remove the accidental loss of collectivity in the γ-vibrational RPA phonons.

between high-spin states using the wave functions in the uniformly rotating frame.[21] Furthermore, one can calculate the $\Delta I=1$ transition rates in odd-mass nuclei by replacement of the Nambu-Goldstone modes which reorient angular momentum of the collective rotation.[8,9] Although this model becomes worse at low-spin states than the particle rotor model because of the one-dimensional cranking approximation and the $1/I$ expansion, it has important merits that the intrinsic model space is larger than, for example, the single-j particle rotor model: We can treat the many-j mixing effect, which is crucial when we treat the natural-parity bands, the quasiparticle-vibration coupling microscopically, and the many-quasiparticle bands on the same footing as the one-quasiparticle bands.

In the present paper we consider the coupling between the odd-quasineutron in natural-parity orbital and the γ vibrational phonons, which gives important effects in the cases of the unique-parity orbitals.[11,12,8,9] The total-state vectors are constructed as the direct products of the internal wave functions and the rotational ones. The internal wave functions consist of the one-quasiparticle components, the one-quasiparticle–one-phonon components, and so on, with respect to the even-even reference states, i.e., the random-phase approximation (RPA) vacua. The effective operators for the transitions between the signature partners are given as follows. The magnetic dipole transition operator is given by

$$\hat{\mu}_{-1}=(g_l-g_{\rm RPA})\hat{l}^{(\rm odd)}_{-1}+(g_s^{(\rm eff)}-g_{\rm RPA})\hat{s}^{(\rm odd)}_{-1} + \sum_n \{[X_n,\hat{\mu}_{-1}]_{\rm RPA}X_n^\dagger-[X_n^\dagger,\hat{\mu}_{-1}]_{\rm RPA}X_n\} , \quad (2)$$

where X_n's represent the RPA phonons. The g factor of the RPA vacuum, $g_{\rm RPA}$, is calculated as

$$g_{\rm RPA}=\frac{\langle\hat{\mu}_x\rangle_{\rm RPA}}{\langle\hat{J}_x\rangle_{\rm RPA}} . \quad (3)$$

Since the reference state for the one-quasiparticle states corresponds to the "rotor," one can regard the $g_{\rm RPA}$, which is slightly $\hbar\omega_{\rm rot}$ dependent in general, as the "g_R." The electric-quadrupole-transition operator is given by

$$\frac{1}{i}\hat{Q}_{-1}=-\sqrt{3/2}\langle Q_0\rangle\frac{\hat{J}_z^{(\rm odd)}}{I_0} +\langle Q_2\rangle\left[2\frac{i\hat{J}_y^{(\rm odd)}}{I_0}+\frac{\hat{J}_z^{(\rm odd)}}{I_0}\right]+\frac{1}{i}\hat{Q}^{(\rm odd)}_{-1} +\sum_n\{[X_n,\frac{1}{i}\hat{Q}_{-1}]_{\rm RPA}X_n^\dagger-[X_n^\dagger,\frac{1}{i}\hat{Q}_{-1}]_{\rm RPA}X_n\}, \quad (4)$$

where $\hat{Q}_{-1}$ and $\langle Q_K\rangle$ ($K=0,2$) are quantized along the rotation axis and the z axis, respectively. The quantity I_0 is the angular momentum of the reference state, which is assumed to be related to the odd-mass-system quantities as

$$I_0=\langle J_x\rangle_{\rm RPA}=I-i_x , \quad (5)$$

where i_x is the aligned angular momentum of the odd quasiparticle.

B. Details of the calculation

The parameters used in the numerical calculations are determined as follows. We used the single-particle space such as the $N_{\rm osc}=4$–6 shells for neutrons and the $N_{\rm osc}=3$–5 shells for protons explicitly, while the contributions from the lower $N_{\rm osc}$ shells are incorporated analytically by assuming the anisotropic-harmonic-oscillator wave functions.[22] Taking into account the isotropic-velocity-distribution condition[22] and the pairing-force strength given in Ref. 9, we obtained $\beta^{(\rm pot)}=0.258$, $\gamma^{(\rm pot)}=0°$, $\Delta_n'=1.07$ MeV, $\Delta_p=1.10$ MeV, and also the chemical potentials which gave the correct particle number at $\hbar\omega_{\rm rot}=0$. The doubly-stretched-quadrupole-force strength[23] is fixed at $\hbar\omega_{\rm rot}=0$ so as to reproduce the excitation energies of the lowest $K=0$ and 2 vibrational states in the neighboring even-even nuclei[24] and to restore the broken rotational invariance. These parameters are used for each spin value, i.e., each frequency $\hbar\omega_{\rm rot}$. The γ-vibrational modes are constructed by the RPA at each frequency; and then the couplings between the odd quasineutron and the γ vibrations are diagonalized. This diagonalization was carried out in the space including up to two-phonon states. We adopted the effective spin g factor $g_s^{(\rm eff)}=0.7g_s^{(\rm free)}$.

Taking account of the driving force due to the odd quasineutron,[25] we calculated equilibrium triaxial deformation for the odd-mass system using the method of Ref. 22. The resulting deformation is $0°<\gamma<3°$ in the frequency range covering the experimental data. Note that the sign of γ is defined opposite to the Lund convention.[26] We used the equilibrium shape of the even-even core; the effects of the odd quasiparticle show up through the particle-vibration coupling. The resulting γ for the even-even core is as small as that for the odd-mass system. These values of γ are smaller than the typical value of the zero-point amplitude in this mass region,[24] $\gamma_0\sim 10°$. Actually the effects of such small γ values on transition probabilities and signature splitting of quasiparticle energy are small. So we take into account only the effects of the dynamical triaxial deformation. The results of the calculations with and without the γ vibrations are shown in Figs. 5–8.

IV. DISCUSSION

A. Characteristic features of $B(M1)$ and quasiparticle energy

The ground-state rotational band of ^{163}Dy is based on the neutron $\frac{5}{2}[523]$ orbital and the main components come from the $h_{9/2}$ and $f_{7/2}$ states. The experimental $B(M1)$ values are about 2 orders of magnitude smaller than those in the $i_{13/2}$ and the $h_{11/2}$ orbital bands.[1–7] This indicates a predominant $j=l-\frac{1}{2}$ character for the band in ^{163}Dy. Furthermore, while the experimental energy splitting is small (Fig. 8), the sign of this splitting is consistent with the single-j model for $j-\frac{1}{2}=$even.[8,9,14]

These experimental results suggest that the main component of the ground-state rotational band is $h_{9/2}$. Note that although the neutron $\frac{5}{2}$[523] Nilsson orbital is adiabatically connected to the $f_{7/2}$ shell-model state in the low-deformation region as stated in a previous paper,[13] the $h_{9/2}$ component becomes dominant in the well-deformed region after an avoided crossing happens.[20]

In the single-j model, signature dependence of the $B(M1)$ and the signature splitting of the quasiparticle energy, ΔE, are correlated[14] in such a way that $B(M1)$ from favored states are enhanced. This selection rule comes from the fact that the $M1$ operator μ is proportional to the angular-momentum operator **J**. Actually it holds well in the case of the unique-parity orbitals such as $\nu i_{13/2}$ and $\pi h_{11/2}$.

Figure 5 shows that the experimental $B(M1)$ values have a relatively strong signature dependence. The single-j model predicts that the $B(M1)$ values of the transitions $I_i=j+2n\rightarrow I_f=j+2n-1$, where n is an integer, become larger than those of the transitions $I_i=j+2n+1\rightarrow I_f=j+2n$. This model, however, has turned out to break down when applied to the present main component, i.e., $j=\frac{9}{2}$.

B. Microscopic analysis of $B(M1)$ and quasiparticle energy

Our rotating-shell-model calculation reproduces not only the unexpected signature dependence of the $B(M1)$ observed but also the sign of signature splitting of the quasiparticle energy simultaneously. The matrix elements of $\hat{J}_z$ and $i\hat{J}_y$ between the lowest-energy natural-parity signature-partner states [we denote them as $J_z(\bar{1}1)$ and $iJ_y(\bar{1}1)$ hereafter] have the same sign, which is consistent with the $h_{9/2}$ character. Since the $M1$-transition rates in the rotating shell model are given by

$$B(M1;r=\mp i\rightarrow\pm i)=\tfrac{1}{2}|\pm i\mu_y(\bar{1}1)+\mu_z(\bar{1}1)|^2\ , \qquad (6)$$

the observed signature dependence of the $B(M1)$ cannot be reproduced if μ is simply proportional to **J**. Actually $i\mu_y(\bar{1}1)$ and $\mu_z(\bar{1}1)$, which includes the j-mixing effects, have the opposite sign in our calculation. To see the detailed mechanism we decompose the matrix elements into orbital and spin contributions. As is shown in Table II, the orbital contribution is larger than the spin contribution in the z component while the latter is larger in the y component; and both contributions have the destructive coherence due to the $\Omega=\Lambda-\frac{1}{2}$ character. This is the reason why the signature dependence of the $B(M1)$ is inverted. More detailed investigation about the $B(M1)$ in natural-parity rotational band will be published separately.[27]

The absolute values of the $B(M1)$ in the rotating shell model are determined by the quantity $|g_j-g_{\rm RPA}|$, where g_j is the Schmidt value for the main component j. The theoretical $B(M1)$ values without the vibrational effects (broken line in Fig. 5) are somewhat larger than the experimental ones. The γ-vibrational effects apparently improve the result (solid line in Fig. 5) at high spins without using the phenomenological g_R. This improvement is mainly due to the second-order perturbation because the $M1$-transition amplitudes associated with the γ-vibrational phonon, $|[\hat{O},X^\dagger_\gamma]_{\rm RPA}|$ where $\hat{O}=i\hat{\mu}_y$ and $\hat{\mu}_z$, in the first-order contribution, are very small. The second-order perturbation brings other single-particle states, which generally have different Ω, into the zeroth-order wave function. It should be pointed out that the calculated $g_{\rm RPA}$ (about 0.34) is larger than the phenomenological value $g_R=0.27$,[28] that is simply determined from experimental values of $(g_K-g_R)/Q_0$ combined with experimental values of the magnetic moment of the ground state and Q_0 of the first excited state from Coulomb excitation.

The signature splitting of the quasiparticle energy is improved at the same time when the γ vibrations are taken into account (see Fig. 8). This holds also for high-j orbitals.[9]

C. Electric quadrupole transitions

Measured and calculated $B(E2)$'s are presented in Figs. 6 and 7. Measured $B(E2)$'s show almost no signature dependence and their absolute values are well reproduced in the rotating shell model (broken lines). This indicates that the adopted shape parameters, β and γ ($\approx 0°$), are appropriate.

Signature dependence of the $B(E2;I\rightarrow I-1)$ has been discussed as the most sensitive probe of the triaxiality in high-j cases.[29] The effect of dynamic triaxial deformation on the $B(E2;I\rightarrow I-1)$ appears in the first-order coupling with the $r=-1$ phonon. The coupling strength is determined by the product of the single-particle matrix element and the RPA transition amplitude $Q_2^{(-)}(\bar{1}1)\cdot[Q_2^{(-)},X^\dagger_\gamma]_{\rm RPA}$. Since $Q_2^{(-)}(\bar{1}1)$ is very small in this nucleus [for example, $Q_2^{(-)}(\bar{1}1)/Q_1^{(-)}(\bar{1}1)\simeq 1/60$ at $\hbar\omega_{\rm rot}=0.183$ MeV], the coupling with the γ vibration has almost no effects on the $B(E2;I\rightarrow I-1)$.

Gamma-vibrational effects on the $B(E2;I\rightarrow I-2)$ are usually small except for the case of very soft nuclei be-

TABLE II. Orbital and spin contributions to angular momentum and magnetic-dipole matrix elements between ground-state signature-partner states at $\hbar\omega_{\rm rot}=0.183$ MeV.

		y component				z component	
il_y	0.110	$(g_l-g_{\rm RPA})il_y$	−0.038	l_z	2.51	$(g_l-g_{\rm RPA})l_z$	−0.86
is_y	−0.0185	$(g_s^{(\rm eff)}-g_{\rm RPA})is_y$	0.056	s_z	−0.23	$(g_s^{(\rm eff)}-g_{\rm RPA})s_z$	0.69
iJ_y	+	$i\mu_y$	+	J_z	+	μ_z	−

cause the contribution from the expectation value $\langle Q_0 \rangle$ is dominant. The one-phonon contribution to the $B(E2;I \rightarrow I-2)$ is only about 1 percent in this case.

V. SUMMARY

We studied electromagnetic properties of the ground-state rotational band of ^{163}Dy based on the $\frac{5}{2}$[523] Nilsson orbital. A significant signature dependence was observed in the $B(M1;I \rightarrow I-1)$ values but not in the excitation energies nor in the $B(E2)$ values. The signature splitting of quasiparticle energy and the absolute values of the $B(M1)$ indicate predominant $h_{9/2}$ character for the ground-state rotational band. On the other hand, signature dependence (zigzag) of the $B(M1)$ shows an unexpected pattern such that transitions from unfavored states are enhanced. We have clarified the microscopic origin of this phenomenon on the basis of the rotating shell model: The phase of the signature dependence of the $B(M1)$ depends on the relative signs of the orbital and the spin contributions.

Coupling with the γ-vibrational excitations improves the absolute values of the $B(M1)$ and ΔE simultaneously. Especially the particle-vibration coupling makes it possible to reproduce the experimental $B(M1)$ at high-spin states without using the phenomenological g_R. Electric-quadrupole-transition probabilities do not show any signature dependence and their absolute values are well reproduced already in the rotating shell model without assuming triaxiality. Coupling with the γ-vibrational phonons does not affect the $B(E2)$'s significantly.

ACKNOWLEDGMENTS

We are grateful to Dr. S. Iwasaki and Dr. A. Ikeda for valuable discussions. We are indebted to Prof. K. Matsuyanagi and Dr. Y. R. Shimizu for fruitful discussions and help in the theoretical calculation. Computer calculation was performed using FACOM M-380 at the Institute for Nuclear Study, University of Tokyo. We would also like to thank Dr. N. Shikazono, Dr. M. Ishii, and Dr. H. Kamitsubo for their support of this study. This study has been carried out as a joint research program between Japan Atomic Energy Research Institute (JAERI) and RIKEN.

*Now at Japan Atomic Energy Research Institute, Tokai, Ibaraki 319-11, Japan.

[1]J. Kownacki, J. D. Garrett, J. J. Gaardhøje, G. B. Hagemann, B. Herskind, S. Jónsson, N. Roy, H. Ryde, and W. Waluś, Nucl. Phys. **A394**, 269 (1983).

[2]G. B. Hagemann, J. D. Garrett, B. Herskind, J. Kownacki, B. M. Nyakó, P. L. Nolan, and J. F. Sharpey-Schafer, Nucl. Phys. **A424**, 365 (1984).

[3]M. Ohshima, E. Minehara, M. Ishii, T. Inamura, and A. Hashizume, Nucl. Phys. **A436**, 518 (1985).

[4]M. Oshima, E. Minehara, S. Ichikawa, H. Iimura, T. Inamura, A. Hashizume, and H. Kusakari, Phys. Rev. C **37**, 2578 (1988).

[5]S. Jónsson, J. Lyttkens, L. Carlén, N. Roy, H. Ryde, W. Waluś, J. Kownacki, G. B. Hagemann, B. Herskind, J. D. Garrett, and P. O. Tjøm, Nucl. Phys. **A422**, 397 (1984).

[6]J. Gascon, P. Taras, D. C. Radford, D. Ward, H. R. Andrews, and F. Banville, Nucl. Phys. **A467**, 539 (1987).

[7]C.-H. Yu, M. A. Riley, J. D. Garrett, G. B. Hagemann, J. Simpson, P. D. Forsyth, A. R. Mokhtar, J. D. Morrison, B. M. Nyakó, J. F. Sharpey-Schafer, and R. Wyss, The Niels Bohr Institute Report TAL88:1 (1988).

[8]M. Matsuzaki, Y. R. Shimizu, and K. Matsuyanagi, Prog. Theor. Phys. **77**, 1302 (1987).

[9]M. Matsuzaki, Y. R. Shimizu, and K. Matsuyanagi, Prog. Theor. Phys. **79**, 836 (1988).

[10]I. Hamamoto and B. R. Mottelson, Phys. Lett. **132B**, 7 (1983).

[11]A. Ikeda, Nucl. Phys. **A439**, 317 (1985).

[12]N. Onishi, I. Hamamoto, S. Åberg, and A. Ikeda, Nucl. Phys. **A452**, 71 (1986).

[13]E. Minehara, M. Oshima, S. Kikuchi, T. Inamura, A. Hashizume, and H. Kumahora, Phys. Rev. C **35**, 858 (1987).

[14]I. Hamamoto, Phys. Lett. **106B**, 281 (1981); in *Proceedings of the Niels Bohr Centennial Conference on Nuclear Structure, Copenhagen, 1985*, edited by R. Broglia, G. B. Hagemann, and B. Herskind (North-Holland, Amsterdam-London, 1985), p. 129.

[15]A. Tveter and B. Herskind, Nucl. Phys. **A134**, 599 (1969).

[16]P. F. Brown, C. Baktash, J. O'Brien, and J. X. Saladin, Phys. Rev. C **18**, 666 (1978).

[17]D. Ashery, N. Assaf, G. Goldring, A. Sprinzak, and Y. Wolfsón, Nucl. Phys. 77, 650 (1966).

[18]J. M. Dairiki, E. Browne, and V. S. Shirley, Nucl. Data Sheets **29**, 653 (1980).

[19]T. Inamura, F. Kearns, and J. Lisle, Nucl. Instrum. Methods **123**, 529 (1975).

[20]A. Bohr and B. R. Mottelson, *Nuclear Structure* (Benjamin, New York, 1975), Vol. 2.

[21]E. R. Marshalek, Nucl. Phys. **A275**, 416 (1977).

[22]Y. R. Shimizu and K. Matsuyanagi, Prog. Theor. Phys. **71**, 960 (1984).

[23]T. Kishimoto, J. M. Moss, D. H. Youngblood, J. D. Bronson, C. M. Rozsa, D. R. Brown, and A. D. Bacher, Phys. Rev. Lett. **35**, 552 (1975).

[24]Nucl. Data Sheets **44**, 659 (1985); **47**, 433 (1986).

[25]S. Frauendorf and F. R. May, Phys. Lett. **125B**, 245 (1983).

[26]G. Andersson, S. E. Larsson, G. Leander, P. Möller, S. G. Nilsson, I. Ragnarsson, S. Åberg, R. Bengtsson, J. Dudek, B. Nerlo-Pomorska, K. Pomorski, and Z. Szymański, Nucl. Phys. **A268**, 205 (1976).

[27]M. Matsuzaki, Phys. Rev. C (to be published).

[28]F. Boehm, G. Goldring, G. B. Hagemann, G. D. Symons, and A. Tveter, Phys. Lett. **22B**, 627 (1966).

[29]M. Matsuzaki, Nucl. Phys. A (in press), and references therein.